Available online at www.sciencedirect.com
SCIENCE DIRECT®
ELSEVIER
Applied Surface Science xxx (2006) xxx–xxx
applied surface science
www.elsevier.com/locate/apsusc

Mechanical properties and the evolution of matrix molecules in PTFE upon irradiation with MeV alpha particles

Gregory L. Fisher [a,*], Rollin E. Lakis [a], Charles C. Davis [a], Christopher Szakal [b], John G. Swadener [c], Christopher J. Wetteland [c], Nicholas Winograd [b]

[a] *Nuclear Materials Technology (NMT-16), Los Alamos National Laboratory, P.O. Box 1663, Los Alamos, NM 87545, United States*
[b] *Department of Chemistry, The Pennsylvania State University 104, Chemistry Building, University Park, PA 16802, United States*
[c] *Materials Science and Technology (MST-8), Los Alamos National Laboratory, P.O. Box 1663, Los Alamos, NM 87545, United States*

Received 29 November 2005; accepted 2 February 2006

Abstract

The morphology, chemical composition, and mechanical properties in the surface region of α-irradiated polytetrafluoroethylene (PTFE) have been examined and compared to unirradiated specimens. Samples were irradiated with 5.5 MeV $^4He^{2+}$ ions from a tandem accelerator to doses between 1×10^6 and 5×10^{10} Rad. Static time-of-flight secondary ion mass spectrometry (ToF-SIMS), using a 20 keV C_{60}^+ source, was employed to probe chemical changes as a function of α dose. Chemical images and high resolution spectra were collected and analyzed to reveal the effects of α particle radiation on the chemical structure. Residual gas analysis (RGA) was utilized to monitor the evolution of volatile species during vacuum irradiation of the samples. Scanning electron microscopy (SEM) was used to observe the morphological variation of samples with increasing α particle dose, and nanoindentation was engaged to determine the hardness and elastic modulus as a function of α dose.

The data show that PTFE nominally retains its innate chemical structure and morphology at α doses $<10^9$ Rad. At α doses $\geq 10^9$ Rad the polymer matrix experiences increased chemical degradation and morphological roughening which are accompanied by increased hardness and declining elasticity. At α doses $>10^{10}$ Rad the polymer matrix suffers severe chemical degradation and material loss. Chemical degradation is observed in ToF-SIMS by detection of ions that are indicative of fragmentation, unsaturation, and functionalization of molecules in the PTFE matrix. The mass spectra also expose the subtle trends of crosslinking within the α-irradiated polymer matrix. ToF-SIMS images support the assertion that chemical degradation is the result of α particle irradiation and show morphological roughening of the sample with increased α dose. High resolution SEM images more clearly illustrate the morphological roughening and the mass loss that accompanies high doses of α particles. RGA confirms the supposition that the outcome of chemical degradation in the PTFE matrix with continuing irradiation is evolution of volatile species resulting in morphological roughening and mass loss. Finally, we reveal and discuss relationships between chemical structure and mechanical properties such as hardness and elastic modulus.

PACS: 61.80.Jh (ion radiation effects); 81.40.Wx (radiation treatment)

Keywords: ToF-SIMS; PTFE; Nanoindentation; Alpha particle; Ionizing radiation

1. Introduction

Interest in the mechanical properties of polytetrafluoroethylene (PTFE) exposed to an alpha (α) radiation field has increased in recent years. This attention was precipitated by an event wherein a PTFE valve seal was implicated as a contributing factor to the unexpected release of $^{238}PuO_2$ inside a room of the Plutonium Facility at the Los Alamos National Laboratory [1]. The release was confined to one room of the facility and did not represent a health risk to the public. Owing to the widespread use of valves with PTFE seals throughout the facility, a study was initiated to determine the suitability of PTFE as a sealing material in a radiological environment. Specifically at issue are the effects that 5.5 MeV α particles, a result of ^{238}Pu decay, have on the mechanical properties of PTFE. It follows that a clear understanding of the chemical properties aids in fully understanding and predicting the mechanical properties.

* Corresponding author.
E-mail address: glfisher@lanl.gov (G.L. Fisher).

0169-4332/$ – see front matter © 2006 Published by Elsevier B.V.
doi:10.1016/j.apsusc.2006.02.002

Many articles appear in the literature regarding the effects of ionizing radiation, including X-ray, gamma (γ), neutron (n) and beta (β) sources, on the chemical and physical properties of PTFE and have been summarized [2–4]. Such radiation fields are typical of those commonly encountered in nuclear reactor, materials processing, and certain analytical environments. Conversely, there is a notable lack of studies probing the chemical and physical properties of PTFE in an alpha (α) radiation field which, arguably, is the dominant radiation field encountered in nuclear production and processing facilities. This lack of data concerning the effects of α radiation on PTFE has led to the inappropriate use of failure doses from other radiation sources to anticipate the failure dose of PTFE in a α particle field or to the use of the lowest known failure dose as a failsafe [1,5,6]. For example, early research indicated a markedly negative impact on the mechanical properties of PTFE following exposure of the sample to thermal neutrons which penetrated the entire thickness of the sample. The exposure threshold of 10^4 Rad was defined by a 25% decrease in elongation-to-failure in a bulk tensile test. In contrast to penetrating sources of radiation, the range of 5.5 MeV α particles in PTFE is ∼27 μm [7], constraining the radiation-induced damage to a very small fraction of the sample cross-section. In the case of α-irradiated PTFE, the properties of the undamaged polymer would dominate the measurement in a bulk tensile test. Therefore, component failure must be defined in terms other than the results of mechanical testing alone.

Radiation induced damage on a total energy basis cannot be extrapolated between radiation sources because damage processes at both the molecular and the bulk scales are incommensurate. High linear energy transfer (LET) sources, such as MeV α particles, deposit more energy in shorter distances creating more reaction centers per unit volume than low LET sources, such as X-ray, γ, n and β radiation, which tend to generate isolated reaction centers [8]. Additionally, the stopping of low mass, high energy ions such as MeV α particles is dominated by electronic interactions (i.e. ionization, bond breaking) while nuclear interactions (i.e. atomic displacement) only become non-trivial at the end of the particle trajectory. Calculation of the range and the LET using SRIM® illustrates that the range of 5.5 MeV α particles in PTFE is on the order of 27 μm and that nuclear stopping only becomes appreciable at ∼24 μm from the surface [7]. The calculations further indicate that nuclear stopping accounts for approximately 2.7% of the total deposited energy with the balance being expended in electronic stopping. For the purposes of our investigations, the effects of nuclear interactions may be neglected. In the surface region, defined as the outer 5 nm, the LET is approximately 0.015% of the total deposited energy which is sufficient to affect a demonstrable change in the chemical composition.

We recently investigated the effects of MeV α particle irradiation on the chemical properties of PTFE using time-of-flight secondary ion mass spectrometry (ToF-SIMS) [7]. The data revealed increased crosslinking, branching, and unsaturation to α doses to $\sim 10^9$ Rad followed by increased fragmentation and unsaturation at α doses above $\sim 10^{10}$ Rad. The evolution of molecular structure in the polymer matrix was accompanied by ingrowth of functionalized perfluoropolyenes. Cleavage of C–F bonds is the mechanism espoused in much of the literature attempting to explain the degradation and functionalization of PTFE upon exposure to ionizing radiation because caging is presumed to result largely in geminal recombination of the $C^{\bullet}$ radicals from main chain scission [4]. However, scission of C–C bonds is thermodynamically favorable and may occur via two mechanisms, direct radiolytic cleavage and homolytic cleavage by $F^{\bullet}$ free radicals. Cleavage of C–C bonds is supported by our observation of crosslinking at moderate levels of irradiation with MeV α particles. The ability of a polymer to crosslink depends on radicals existing in both spatial and temporal proximity, a condition that usually requires a high LET interaction [8]. The requirement for spatial and temporal proximity of radicals is met during irradiation of PTFE with total fluences of MeV α particles in the range of 10^{11} to 10^{15} cm^{-2}, corresponding to experimental doses of 10^7 to 10^{11} Rad. Moreover, the structural degradation of PTFE via MeV α particle irradiation appears to be cumulative and continuous which is a direct consequence of the range and complete transfer of energy from the incident particles to matrix molecules. While MeV α particles have a decidedly limited range in the polymer, deterioration with continuous irradiation is apparently brought about by fragmentation, functionalization, and gas evolution. As we will explore further in this article, the aforementioned processes lead to roughening of the surface which exposes further material to the incident radiation.

In our previous report we acknowledged the necessity for further investigation into the degradation of α-irradiated PTFE using more sensitive surface probes and performing analysis of evolved gases. We report here our most recent results using ToF-SIMS, scanning electron microscopy (SEM), residual gas analysis (RGA), and nanoindentation to characterize the cumulative effects of MeV α particles on a PTFE matrix. To our knowledge, the data presented herein represent the first systematic effort to correlate chemical and mechanical properties as a function of radiation exposure. These results corroborate previous conclusions and extend our understanding of the effects of α particle irradiation on PTFE.

We have revisited the ToF-SIMS analysis of α-irradiated PTFE using a custom instrument equipped with a 20 keV C_{60}^+ primary ion source. ToF-SIMS analysis of polymers using a C_{60}^+ ion probe offers several analytical advantages over use of a $^{69}Ga^+$ ion probe, as evidenced in our data. We have observed a minimum 500-fold increase in signal over previous data sets, illustrated in Fig. 1, substantiated by a multiplication of 50 or better in total ion counts acquired using an order of magnitude less total ion dose. The reduction in primary ion current has also enabled the collection of mass spectra in the negative polarity at each radiation dose, as shown in Fig. 2. Additionally, we have observed higher and more consistent mass resolution allowing unambiguous identification of isobaric species. The increases in signal and mass resolution, together with the minimization of charging artifacts, have facilitated the assignment of fragments to a mass-to-charge (m/z) ratio of 300 m/z. These factors have also enabled the acquisition of ion-specific images with which

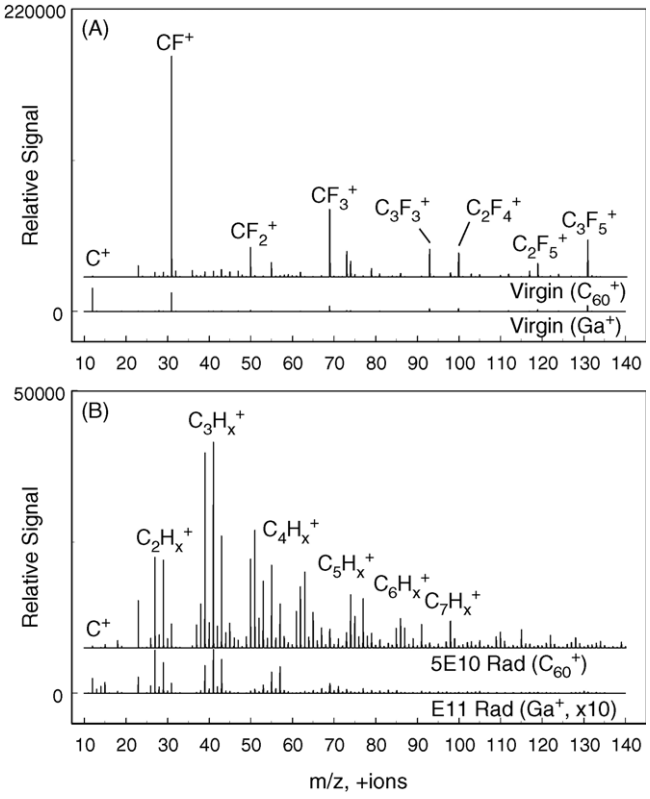

Fig. 1. Positive SIMS spectra of PTFE prior to and following irradiation by 5.5 MeV α particles acquired using $^{69}Ga^+$ and C_{60}^+ primary ions. (A) The 10–140 *m/z* region of mass spectra acquired at zero dose. (B) The 10–140 *m/z* region of mass spectra acquired at the maximum radiation dose. Characteristic PTFE fragment ions are indicated by formula in the spectra acquired at zero dose and prominent hydrocarbon moieties are indicated by formula in the spectra acquired at the maximum radiation dose. The signal of the mass spectrum acquired from PTFE irradiated to 10^{11} Rad using $^{69}Ga^+$ primary ions is multiplied by 10.

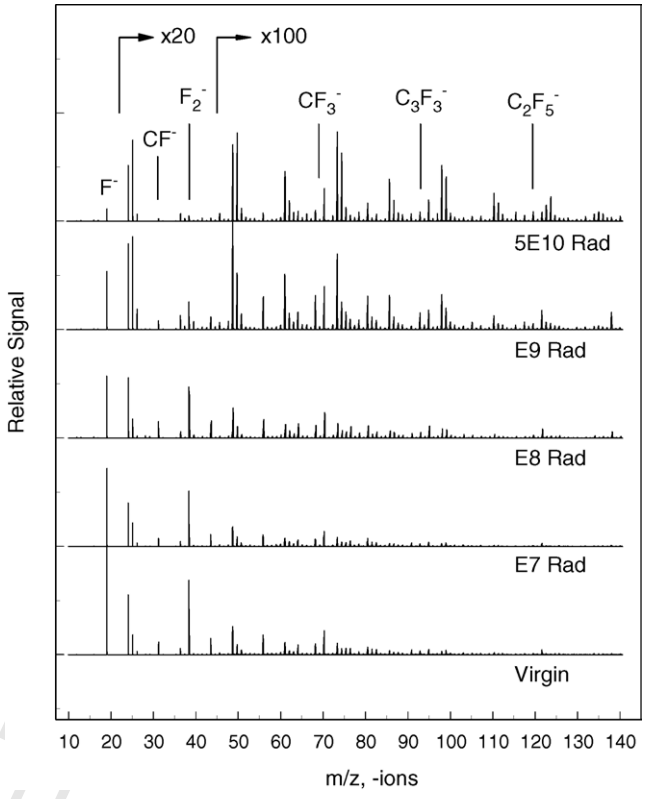

Fig. 2. Stacked negative SIMS spectra of PTFE showing the 10–140 *m/z* region prior to and following irradiation by 5.5 MeV α particles. Characteristic PTFE fragment ions are indicated by formula. The signals of the mass spectra are multiplied by 20 at *m/z* ≥20 and are multiplied by 100 at *m/z* ≥45.

to identify chemical features and trends in the mass spectra as a direct consequence of α particle irradiation. This considerable increase in both quality and volume of ToF-SIMS data has revealed additional information regarding the chemical properties of α-irradiated PTFE and are given in conjunction with SEM, RGA, and physical property data.

2. Experimental

2.1. Sample preparation

Neat PTFE in 2 mm thick sheets, purchased from Goodfellow (Berwyn, PA, USA, P/N FP303100), and valve seal material having 15% by volume fiberglass content in a DuPont® T7 matrix were used in these experiments. Nitrile gloves were donned prior to handling samples, and all manipulation was accomplished with methanol-cleaned and nitrogen-dried tools. Neat PTFE specimens were cut from the sheet stock for subsequent irradiation. Valve seal material was removed from new valves, cleaned, cut to appropriate dimensions, and polished on one side using standard metallographic techniques prior to mounting and irradiation.

Once the sample was mounted in the holder, it was introduced into the vacuum vessel for irradiation. The irradiation chamber is attached to the tandem accelerator beam line, but separated from it by several skimmed differential pumping stations. The irradiation chamber vacuum system consists of a 510 L/s turbopump backed by a mechanical pump. A pressure of $<1 \times 10^{-6}$ Torr was achieved before irradiation of each sample. As determined by RGA, the background was comprised of common vacuum contaminants of H_2, H_2O, CO/N_2, O_2, and CO_2 at partial pressures commensurate with the total pressure.

2.2. Alpha irradiation

The damage imparted to PTFE by ^{238}Pu-generated α particles was simulated by irradiating the sample with 5.5 MeV $^4He^{2+}$ particles generated in a tandem accelerator beam line. The samples were exposed to a ~0.3 cm diameter continuous (DC) beam that was scanned over the exposed portion of the sample. All samples were nominally maintained at room temperature during irradiation. The neat PTFE samples were irradiated to nominal α doses of 10^7, 10^8, 10^9, 10^{10}, and 5×10^{10} Rad, and the 15% glass content PTFE samples used for nanoindentation were irradiated to nominal α doses of 10^6, 5×10^6, 10^7, 5×10^7, 10^8, 5×10^8, 10^9, 5×10^9, and 10^{10} Rad. For comparison, 1 Rad is equivalent to 0.01 gray (Gy) and 100 erg/g. Beam currents were typically 0.2 nA at a

dose of 10^6 Rad, 5 nA for doses between 10^7 and 10^8 Rad, 15 nA at a dose of 10^9 Rad, and 25 nA for doses $\geq 10^{10}$ Rad. Samples used during RGA were irradiated at a beam current of 40 nA. As shown previously, samples irradiated at different dose rates have been found to be indistinguishable [7]. Irradiation was performed in continuous fashion for each nominal dose. The relative error in the cumulative dose measurements is ±10%. Following irradiation, the samples were pulled from the irradiation chamber, loaded into wafer holders, and stored in ambient conditions for subsequent analysis.

2.3. Gas analysis

Evolution of fluorocarbon species, as well as CO/N_2, O_2, and CO_2, was monitored during irradiation with a quadrupole-based residual gas analyzer (Stanford Research Systems, Sunnyvale, CA, USA, P/N RGA200). The pressure versus time scans were performed under the conditions of a 1 mA emission current, a 70 V accelerating voltage, a gain of approximately 1000, and a 1 s sampling period. The ionizer of the RGA was positioned approximately 7 in. from the specimen during analysis, and was not mounted within line-of-sight of the samples. The thoriated iridium filaments were thoroughly degassed prior to experimental data acquisition. Species with nominal masses corresponding to HF^+, CF^+, F_2^+, and CF_3^+ were monitored concurrently during irradiation of the samples.

2.4. ToF-SIMS analysis

Surface analysis of the neat PTFE specimens by ToF-SIMS was performed using a custom instrument, detailed elsewhere [9], approximately two weeks following irradiation. The system is equipped with a sorption-pumped chamber for fast sample introduction to a turbo-pumped antechamber, and an ion-pumped analysis chamber with a base pressure of $<1 \times 10^{-9}$ Torr. Nitrile gloves were donned prior to handling samples, and all manipulation was accomplished with methanol cleaned and air dried tools. The samples were mounted on the sample holder and introduced into the turbo-pumped antechamber via the fast sample entry. The antechamber was pumped down to $<1 \times 10^{-6}$ Torr before the samples were transferred to the analytical chamber. Secondary ions for mass spectral and chemical image acquisition were generated using a 20 keV C_{60}^+ ion source focused to a diameter of $\leq$30 μm at the sample [10]. During data acquisition the primary ion beam conditions were a pulsewidth of 50 ns at 3 kHz and a DC current of 0.54 nA. The raster area was 200 μm × 200 μm during spectrum acquisition, and 400 μm × 400 μm during imaging. Mass spectra were acquired with the raster area completely within or outside the irradiated portion of the sample, while images were always collected at the boundary of the irradiation zone. In the course of spectrum acquisition approximately 2.7×10^{11} C_{60}^+ cm^{-2} impinged the surface of the analytical area, an order of magnitude below the static limit [11]. The total ion dose during imaging was one-fourth the total ion dose used for spectrum acquisition. Analyses were performed with a nominal mass resolution ($m/\Delta m$) of ~2500 in the mass-to-charge (m/z) region below 100 m/z. The mass resolution in the negative polarity was <500 in the same mass-to-charge range. No charge compensation was required during spectrum or image acquisition.

Mass spectra were collected from the unirradiated and α-irradiated portions of the sample in the mass-to-charge (m/z) range of 4–1800 m/z in both the positive and negative polarities. In general, the total counts of the negative ion spectra are generally less than 1/16 the total counts of the corresponding positive ion spectra. A total of three neat PTFE samples were analyzed. Each sample included the α radiation doses described in Section 2.2. Within each zone at least two different areas were analyzed. A single image was acquired at the boundary of each irradiation zone of each sample. For mass spectral features related to the polymer matrix, relative peak intensities were generally reproducible to within ±20% from sample to sample. Where quantitative correlations are made, measurements from all samples were used to determine the mean and standard deviation of the measurement. Data values greater than one standard deviation (1σ) from the estimated mean were excluded from the data set, and the mean was calculated using a minimum of three data points for each measurement. Statistically anomalous data points are straightforwardly attributed to sample-to-sample variation, and morphological roughness at α doses $>10^9$ Rad, since sample charging was not observed to be a significant obstacle during analysis.

2.5. Scanning electron microscopy

Surface imaging of 15% glass content specimens by SEM was performed using an Hitachi VP-3500N environmental microscope to document the morphological variation of the specimens following irradiation. The instrument is equipped with a Robinson-type electron detector and is capable of high resolution imaging in variable pressure mode. Instrumental conditions during imaging were an accelerating voltage of 15 kV and a probe current of ≤1 nA. Imaging was performed at pressures between 20 and 80 Pa which eliminated the need for a conductive coating or additional specimen preparation.

2.6. Nanoindentation

The hardness and elastic modulus within irradiated regions of the 15% glass content specimens were measured using an MTS NanoII nanoindenter up to three months from the time of irradiation. Nanoindentation, which is indentation at low loads with accurate depth and load measurement, was used to ensure that only the mechanical properties of the damaged surface region (approximately 26 μm in depth) were probed. The specimens were conditioned at 20 ± 1 °C for a minimum of 12 h prior to testing. All indentation locations were selected individually by viewing the specimens at 200× magnification and choosing sites that were free of scratches and fibers over an area at least three times the size of the indent. A minimum of four tests were performed on each specimen.

Indentations were conducted using a Berkovich three-sided pyramidal tip. Displacements and loads were measured with a resolution of 0.04 nm and 0.08 μN, respectively. The indents were run in load control with a feedback system to manage the displacement rate which was gradually increased to a maximum of 64 nm/s and to a maximum total depth of 2560 nm (~2.5 μm). The loading rate was increased proportionally to the depth squared so that the effective strain rate during indentation was kept approximately constant. During indentation, a 45 Hz oscillation with a magnitude of 2 nm peak-to-peak was superimposed on the loading path. The load and displacement signals were fed through a lock-in amplifier so that the contact stiffness was recorded simultaneously with the load and displacement data. The Oliver-Pharr method was used to analyze the nanoindentation data, and the continuous stiffness method was utilized to determine the hardness and elastic modulus acquired during the loading step [12]. Only data from the 45 Hz loading step was analyzed because time-dependent deformation renders data from the constant loading and unloading steps to be of no value.

3. Results

The fingerprint peaks of the unirradiated PTFE are found mostly below 200 *m/z* [13] with a few additional peaks of the characteristic form $[C_nF_{2n-1}]^+$ extending out to 400 *m/z* [14]. In general, we find that the relative intensities of the fingerprint peaks provide a useful indication that the samples have been prepared and handled without significant incorporation of impurities. The mass spectral features of the unirradiated specimens have been described in detail [7]. Upon irradiation, changes in the signal of characteristic PTFE fragments, as well as new features in the mass spectra, were monitored. After the initial radiation dose the signals of characteristic PTFE fragments gradually decrease in intensity with a concurrent increase in the signal of hydrocarbon moieties, an observation that was reported previously [7]. Mass spectra acquired in the positive polarity using $^{69}Ga^+$ and C_{60}^+ primary ions are rendered in Fig. 1 for comparison; the top frame shows the mass spectra at zero dose and the bottom frame shows the mass spectra at the respective maximum doses. The trends in the mass spectra are qualitatively similar, albeit much greater signal levels are achieved with use of the polyatomic primary ion source. The increase in signal levels has also allowed the identification of processing additives such as isoparaffins [15,16], perfluorinated polyether [13], and silicone oil [13] that were not evident in the mass spectra acquired using the monatomic primary ion source.

The negative ion mass spectra in the range of 10–140 *m/z* are plotted as a function of α dose in Fig. 2. The characteristic fragment ions of unirradiated PTFE and their nominal mass-to-charge ratios are F^- (19 *m/z*), CF^- (31 *m/z*), F_2^- (38 *m/z*), CF_3^- (69 *m/z*), $C_3F_3^-$ (93 *m/z*), and $C_2F_5^-$ (119 *m/z*). Distinguishing evidence of silicones in the negative ion spectra includes peaks at 59 *m/z* (CH_3SiO^-), 60 *m/z* (SiO_2^-) and 75 *m/z* ($CH_3SiO_2^-$), while evidence of perfluorinated polyether appears at 61 *m/z* ($C_2H_2FO^-$) and 109 *m/z* ($C_3H_3F_2O_2^-$). The presence of isoparaffins [15,16] is confirmed by a number of hydrocarbon peaks in the negative ion spectra at zero dose.

Upon irradiation of the sample with α particles, the signals of characteristic PTFE fragments decrease with a concomitant rise in the signals of extant and emergent peaks. As noted above in the positive ion mass spectra, the rise in the signals of hydrocarbon moieties is significant. The hydrocarbon signals become more prominent at α doses $\geq 10^9$ Rad, an observation that is illustrated in Fig. 3. The trending of the hydrocarbon species relative to the fluorocarbon species in the negative polarity is represented by the ratio of CH^-/CF^- plotted against the log of the dose. The mean values of the ratio at each α dose were calculated using data from all samples excluding outliers; the error bars indicate an interval of one standard deviation (1σ) from the mean. The data are plotted on a log–linear scale and are fit by a weighted first-order exponential function as a guide to the eye. The divergence in the signals of hydrocarbon and fluorocarbon moieties is minimal at α doses $<10^9$ Rad, whereas at α doses $\geq 10^9$ Rad the divergence in these signals is quite pronounced. The trends in the negative polarity are corroborated by the hydrocarbon and fluorocarbon signals in the positive polarity. The $C_3H_3^+/C_3F_3^+$ ratio is evaluated because

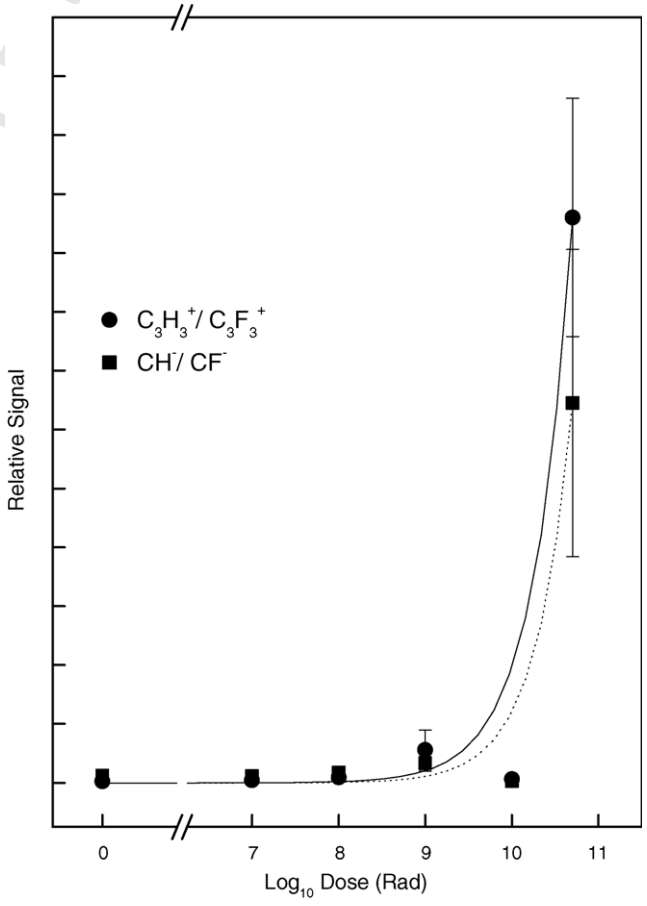

Fig. 3. Hydrocarbon-to-fluorocarbon ratios, $C_3H_3^+/C_3F_3^+$ (●) and CH^-/CF^- (■), plotted against the log of the dose on a log–linear scale. The error bars indicate an interval of one standard deviation ($\pm 1\sigma$) from the mean. The weighted first-order exponential curve fits for both $C_3H_3^+/C_3F_3^+$ (—) and CH^-/CF^- (· · ·) are a guide to the eye.

the C_3 fragments are relatively stable products of sputtering [17,18], and to provide a point of comparison with previous work wherein a monatomic primary ion source was utilized to probe the samples [7]. As observed, these ratios follow remarkably well and are, therefore, used as a reliable gauge of the hydrocarbon-to-fluorocarbon trending. We further conclude that while improvements in signal and mass resolution have been realized using a C_{60}^+ ion probe, along with a reduction of charging artifacts, there are no discernable differences in the detected products of α particle radiolysis.

The signals of several characteristic fragment ions of PTFE from the positive ion mass spectra are presented in Fig. 4. In this figure, the mean of the integrated signals of CF^+, C_3F^+, $C_3F_3^+$, and $C_3F_5^+$ are plotted against the log of the dose. These ions seem ideal indicators of α particle-induced chemical degradation of the polymer matrix because they are stable products of PTFE sputtering [17,18] and because there are no unresolved interferences giving rise to additional error. The mean values were calculated using data from all samples, excluding outliers, and are normalized to the total ion signals at each α dose. The error bars indicate an interval of one standard deviation (1σ) from the mean. The data, plotted on a log–log scale, are fit from 10^7 to 5×10^{10} Rad by the relationship $y = ae^{bx}$ where y is the normalized ion signal and x is the $\log_{10}$ of the dose. The resulting slope and intercept for each curve is CF^+ (−0.279, 8.23×10^6), C_3F^+ (−0.380, 2.87×10^6), $C_3F_3^+$ (−0.397, 8.71×10^6), and $C_3F_5^+$ (−0.698, 8.20×10^7). The linear relationship between radiation dose and fluorocarbon signal is obvious and shows a trend of signal degradation with increasing α particle irradiation.

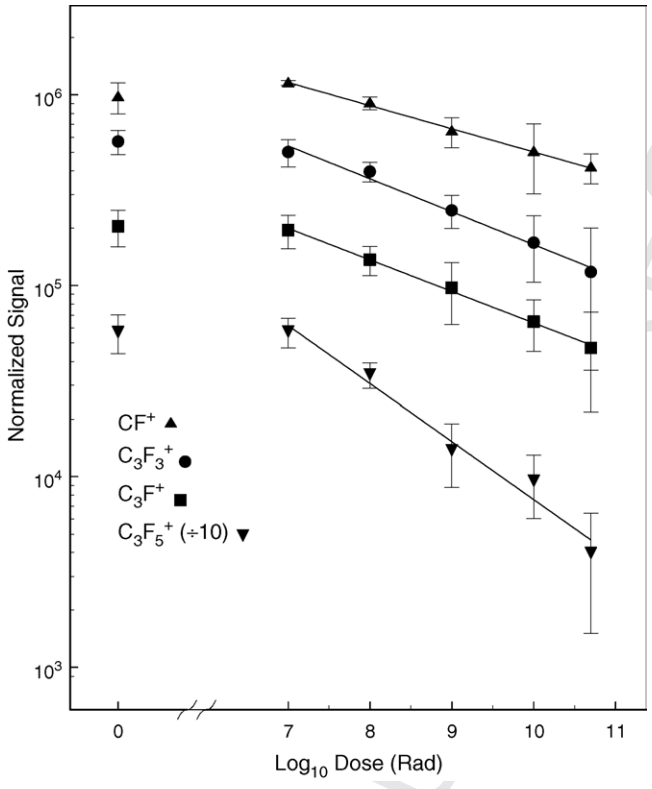

Fig. 4. Integrated signals of the characteristic PTFE fragment ions CF^+ (▲), C_3F^+ (■), $C_3F_3^+$ (●), and $C_3F_5^+$ (▼) plotted against the log of the dose on a log–log scale. The data are normalized to the total ion signal at each dose and are fit by the relationship $y = ae^{bx}$ over the experimental dose range of 10^7 to 5×10^{10} Rad. The resulting slope and intercept for each curve are given in the text. The residuals (R^2) are 0.997 for CF^+, 0.998 for C_3F^+, 0.978 for $C_3F_3^+$, and 0.986 for $C_3F_5^+$. The error bars indicate an interval of one standard deviation ($\pm 1\sigma$) from the mean. The signal of $C_3F_5^+$ has been divided by 10 to eliminate the overlap of data in the figure.

We have made mention of the fact that characteristic PTFE fragments progressively favor defluorinated oligomers (i.e. $[C_nF_{2n-1}]^+$) with increasing α particle irradiation [7]. This supposition is substantiated by the curve fit data shown in Fig. 4. The $C_3F_x^+$ ions are presumed to have similar structures which enhances the direct, quantitative comparison of these ion signals [18]. However, the increasing level of unsaturation present in the $C_3F_x^+$ ions limits the potential for resonance stabilization. For this reason the initial signal levels (i.e. at zero dose) of the $C_3F_x^+$ ions decreases with increasing unsaturation. It should be noted that the signal of $C_3F_5^+$ has been divided by 10 to eliminate overlap of data in the figure. The slope of the curves for C_3F^+, $C_3F_3^+$, and $C_3F_5^+$ are −0.380, −0.397, and −0.698, respectively. These data show that α radiolysis of the polymer matrix results in a bias of detected ions toward unsaturated, or fluorine deficient, species with increasing α dose. This observation might be interpreted as an indication that radiolytic cleavage of C–F and C–C bonds does not occur stochastically; rather, a predisposition toward C–F bond cleavage may be present.

The cumulative degradation of PTFE with continued α particle irradiation, and concomitant proliferation of hydrocarbon and functionalized fluorocarbon species, is further demonstrated by chemical imaging. The ion-specific images of CF^+, $[SiC_2]H^+$, $C_4H_5^+$, CFO_2^+, and $C_3F_5^+$ are displayed in Fig. 5; the total ion images of the positive polarity are provided as a reference to which topographically related artifacts may be compared. Within each image window, the irradiated portion of the sample is to the right and the unirradiated portion of the sample is to the left. Images from the negative polarity are not included because the low signals and poor resolution, as compared to the positive polarity, do not provide additional enlightenment. As evidenced in the total ion images, some degradation of the signals is realized in the irradiated portion of samples and is attributed to surface roughening at high α doses. The CF^+ and $C_3F_5^+$ ion images at 10^9 Rad show demonstrable radiolytic decomposition of the PTFE matrix that increases at higher α doses. Likewise, the $C_4H_5^+$ and CFO_2^+ ion images illustrate that the burgeoning signals of hydrocarbons and functionalized fluorocarbons are an effect of α radiolysis because the increasing signals of these moieties is localized to the irradiated portions of the samples. The $C_4H_5^+$ and CFO_2^+ signals are evident at 10^9 Rad, and escalate with increased α dose. Conversely, ion images of $[SiC_2]H^+$ reveal an ubiquitous signal throughout the irradiation regime. This observation is expected since $[SiC_2]H^+$ is a fragment of silicone residues that are present as a processing residue. It is also worth mentioning that $[SiC_2]H^+$ and $C_4H_5^+$ are isobaric, i.e. having the same nominal mass-to-charge ratio. These isobars are imaged with an acceptable level of contrast as a result of the analytical

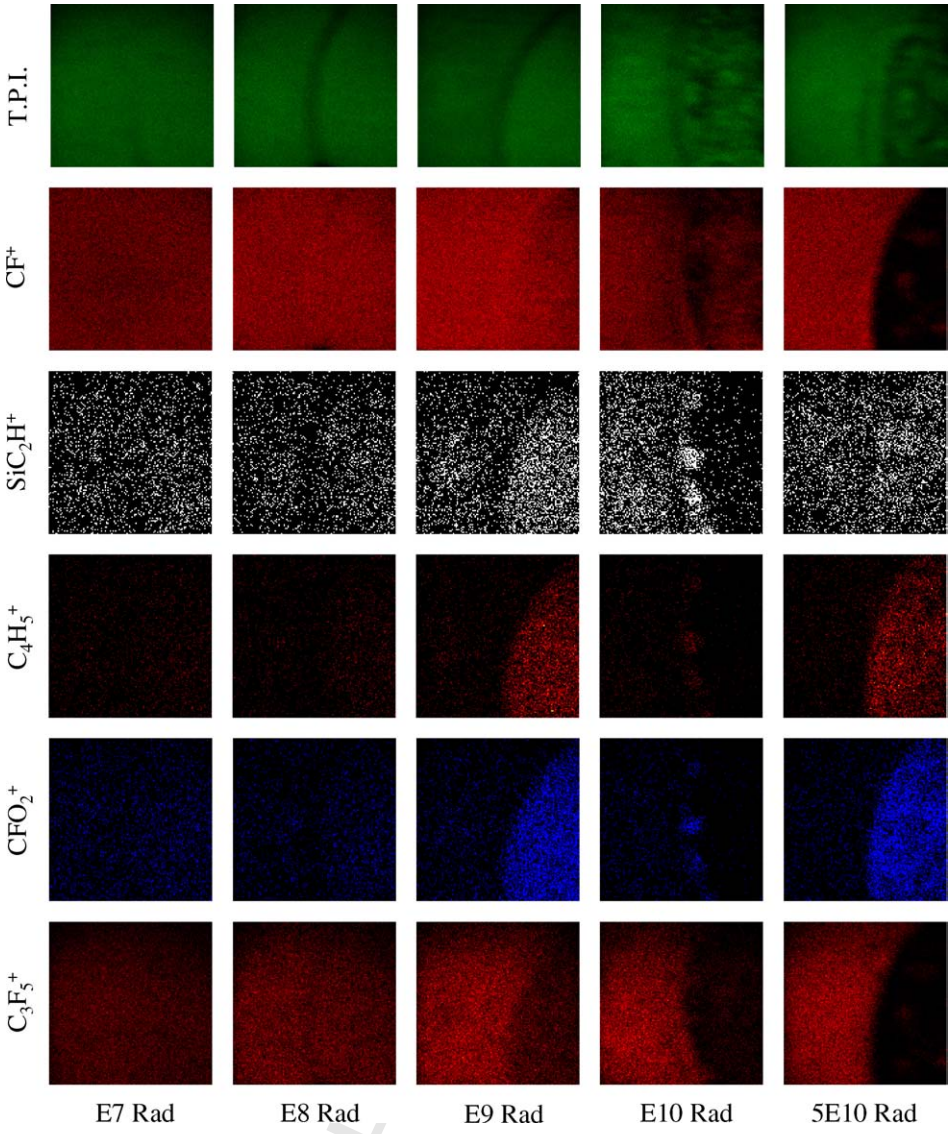

Fig. 5. Positive ion-specific images of α-irradiated PTFE at each experimental dose. Image sizes are 400 μm × 400 μm. Within each image, the irradiated portion of the sample is to the right while the unirradiated portion is to the left. While the signals of emergent species are suppressed within the 10^{10} Rad irradiation zone of all samples ostensibly due to topographical roughness, the signals of extant species appear to be less affected. Images in each row are normalized to the same counts/pixel scale. Row 1: total positive ion (T.P.I.) on a scale of 0–846. Row 2: CF^+ on a scale of 0–75. Row 3: SiC_2H^+ on a scale of 0–1. Row 4: $C_4H_5^+$ on a scale of 0–21. Row 5: CFO_2^+ on a scale of 0–15. Row 6: $C_3F_5^+$ on a scale of 0–60.

advantages afforded by use of the C_{60}^+ ion probe during ToF-SIMS data acquisition. Lastly, the total ion images depict a surface morphology which roughens with increasing α dose. A consequence of surface roughness is suppression of the signals of extant and emergent species, such as $[SiC_2]H^+$, $C_4H_5^+$, and CFO_2^+, ostensibly via termination of the extraction field at topographical maxima. The signals of ions arising from the polymer matrix (e.g. CF^+ and $C_3F_5^+$) are apparently less affected by gradients in the extraction field.

Current and previous ToF-SIMS data suggest that the result of α particle irradiation of PTFE is unsaturation, crosslinking, functionalization and, ultimately, fragmentation of molecules in the polymer matrix. Moreover, ion images reveal morphological roughening of the surface which implies some mass loss from the polymer matrix. The high resolution SEM images pictured in Fig. 6 more clearly illustrate the morphological roughening and mass loss that accompanies high doses of α particles. The SEM specimens are comprised of a DuPont® T7 matrix with a 15% by volume fiberglass content. The fiberglass fill has no demonstrable impact on the radiochemistry [7]. For the purposes of this experiment, the fiberglass fill provides a convenient marker against which to gauge the extent of material loss. At 10^9 Rad there is no discernable change in the surface morphology. It is interesting to note that, while SEM reveals no perceptible change in morphology at 10^9 Rad, a change in the chemistry is revealed by ToF-SIMS. By 10^{10} Rad there is clear evidence of morphological evolution in the form of stress cracks which may be accompanied by mass loss. At α doses in excess of 10^{11} Rad, extreme morphological variation and mass loss is obvious. While there does not appear to be a direct

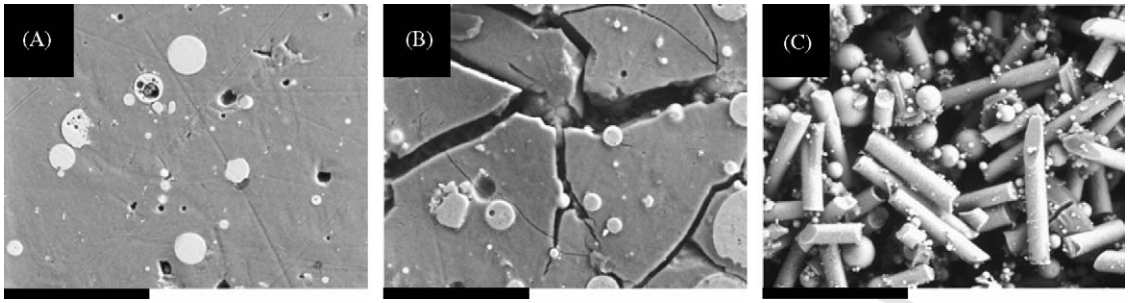

Fig. 6. Scanning electron micrographs of fiberglass-reinforced PTFE that has been exposed to 5.5 MeV α particles. (A) Total dose of 10^9 Rad. (B) Total dose of 10^{10} Rad. (C) Total dose of 10^{11} Rad. The markers indicate 100 μm.

correspondence in the images obtained by SEM and ToF-SIMS, the differences are straightforwardly attributed to the presence or absence of fiberglass in the sample matrices. Even so, both the ToF-SIMS and the SEM images indicate mass loss as a consequence of α particle irradiation at doses $>10^9$ Rad.

The RGA data displayed in Fig. 7 show the partial pressures of evolved gases during the α particle irradiation of PTFE. The samples were irradiated using a beam current of 40 nA which corresponds to a dose rate of 5×10^7 Rad/s. Ions with nominal mass-to-charge ratios corresponding to HF^+ (20 *m/z*), CF^+ (31 *m/z*), F_2^+ (38 *m/z*), and CF_3^+ (69 *m/z*) were monitored during irradiation of the sample. The signal of CO_2^+ (44 *m/z*) was tracked for comparison, and serves as verification that the observed rise in the partial pressures of HF^+, CF^+, F_2^+, and CF_3^+ are caused specifically by radiolysis of the PTFE matrix and are not the result of a systemic error, e.g. induced desorption of physisorbed species on the sample holder. The first appearance of evolved species occurs at 3×10^{10} Rad where a marginal increase in the partial pressure of CF_3^+ is detected. However, at 5×10^{10} Rad several species are evolved from the irradiated sample at significant partial pressures. The sharp rate of rise in the partial pressures of CF^+ and CF_3^+ is accompanied by a more gradual rate of rise in the partial pressures of HF^+ and F_2^+. The baseline of HF^+ is initially elevated and declines as a function of time. This observation may be understood in light of anecdotal evidence which suggests that thoriated iridium filaments behave as getters of fluorine. When the RGA filaments are hot, fluorine is evolved and combines with hydrogen in the ionization region leading to an apparently elevated background of hydrogen fluoride. While the RGA filaments are thoroughly degassed prior to irradiation, not all of the fluorine is liberated and pumped away. Nevertheless, these data unambiguously show the evolution of α particle-generated matrix fragments at high α doses and confirm the suppositions derived from the ToF-SIMS and SEM data.

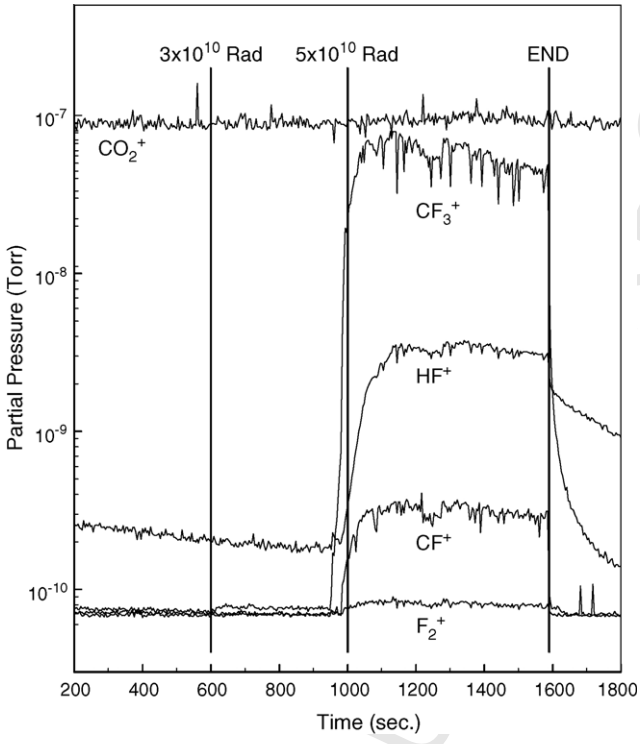

Fig. 7. Residual gas analysis performed during α particle irradiation of PTFE. Traces are shown for HF^+ (19 *m/z*), CF^+ (31 *m/z*), F_2^+ (38 *m/z*), and CF_3^+ (50 *m/z*). The signal of CO_2^+ (44 *m/z*) is shown for comparison, and serves as verification that the observed rise in the partial pressures of HF^+, CF^+, F_2^+, and CF_3^+ are caused by radiolysis and are not the result of a systemic error. The sample was irradiated at a rate of 5×10^7 Rad/s using a beam current of 40 nA. The first appearance of liberated gases is observed at $\sim 3 \times 10^{10}$ Rad, and a significant rise in all signals is observed at $\sim 5 \times 10^{10}$ Rad. Irradiation was terminated at 1580 s.

Relative changes in the polymer structure upon α particle irradiation may be extracted by evaluating subtle trends in the signals that arise from monomer units [19]. Specifically, the signals of $C_2F_5^+$ (monomer + F) and $C_2F_3^+$ (monomer − F) are monitored to reveal changes in the polymer structure as a function of α dose. The mechanism for emission of these analyte species is well founded in the mass spectrometry of long-chain aliphatic homologs [19,20]. In the analysis of low molecular weight polymers, the signals of $C_2F_5^+$ and $C_2F_3^+$ are typically representative of endgroup and bulk monomer signals, respectively [19]. However, PTFE is a high molecular weight polymer wherein each polymer chain is comprised of $\sim 10^5$ monomer units. These circumstances effectively minimize the influence of chain ends on the signal of $C_2F_5^+$. Rather, the signals of $C_2F_5^+$ and $C_2F_3^+$ are composite indicators of the degree of unsaturation, fragmentation, and crosslinking in the polymer matrix. Additionally, the signals of $C_2F_5^+$ and $C_2F_3^+$ do not appear to be affected by unsaturation, fragmentation, and crosslinking to the same proportion. Therefore, the signals of $C_2F_5^+$ and $C_2F_3^+$ must be considered together and evaluated against other data.

In Fig. 8, the ratios of $C_2F_5^+/C^+$ and $C_2F_3^+/C^+$ are plotted as a function of α dose on a log–linear scale. The data are ratioed to C^+ (12 *m*/*z*) since it is a non-specific fragment ion useful for normalization, are fit with a spline curve as a guide to the eye, and are plotted on the same relative scale for ease of comparison. The error bars indicate an interval of one standard deviation (1σ) from the mean. Upon irradiation, the magnitude of the $C_2F_3^+/C^+$ ratio increases slightly to an α dose of 10^8 Rad followed by a significant decline to a dose of 10^{10} Rad and a sharp increase at 5×10^{10} Rad. The rise in the magnitude of the $C_2F_3^+/C^+$ ratio at α doses $\leq 10^8$ Rad is likely an indication of increased unsaturation in the polymer matrix. Likewise, the rise in the magnitude of the $C_2F_3^+/C^+$ ratio at 5×10^{10} Rad is an indication of increased unsaturation. However, severe fragmentation of the polymer matrix undoubtedly contributes to the large magnitude of the $C_2F_3^+/C^+$ ratio at 5×10^{10} Rad. Fragmentation and branching, while not observed to be extensive until $\geq 10^{10}$ Rad, is confirmed by the increasing trend of the CF_3^+/C^+ ratio versus α dose [11,21]. We suggest that the depression in the $C_2F_3^+/C^+$ curve between 10^9 and 10^{10} Rad is the result of crosslinking, occurring by a number of mechanisms, that would effectively reduce the yield of (monomer − F) ions. In similar fashion, the magnitude of the $C_2F_5^+/C^+$ ratio increases to an α dose of 10^{10} Rad, going through a maxima between 10^9 and 10^{10} Rad, followed by an abrupt decline at 5×10^{10} Rad. The increase in the magnitude of the $C_2F_5^+/C^+$ ratio at α doses $\leq 10^{10}$ Rad is likely an indication of increased scissioning of the polymer chains which, in effect, increases the apparent concentration of endgroups. The decline in the magnitude of the $C_2F_5^+/C^+$ ratio at α doses $>10^{10}$ Rad is attributed to α particle-induced defluorination, or unsaturation, of the polymer matrix. The maxima in the $C_2F_5^+/C^+$ curve is coincident with the minima in the $C_2F_3^+/C^+$ curve. We rationalize that a peak in the level of crosslinking at $\sim 5 \times 10^9$ Rad is the source of both the minima in the (monomer − F) ion yield and the maxima in the (monomer + F) ion yield at the same dose. It should be noted that the trends in the magnitudes of the $C_2F_5^+/C^+$ and $C_2F_3^+/C^+$ ratios at 10^7, 10^8, and 10^9 Rad are, for all practical purposes, a straight line (i.e. largely within the experimental error); however, the trends between 10^7 and 10^{10} Rad are real (i.e. greater than the experimental error), and are confirmed by other data. The relative insensitivities of the $C_2F_5^+/C^+$ and $C_2F_3^+/C^+$ ratios to α particle dose at $\leq 10^9$ Rad is likely a real effect of the high molecular weight of the polymer. Likewise, the observed variation in the magnitude of the $C_2F_5^+/C^+$ and $C_2F_3^+/C^+$ ratios at α doses $>10^9$ Rad may be an indication that the average molecular weight of the polymer lies within the ability of the ToF-SIMS technique to distinguish.

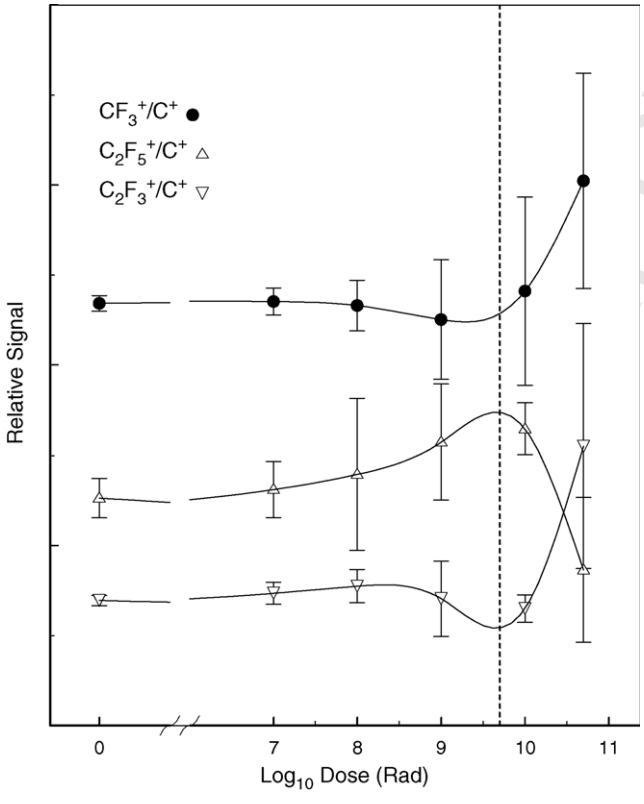

Fig. 8. The magnitudes of the $C_2F_5^+/C^+$ (△), $C_2F_3^+/C^+$ (▽), and CF_3^+/C^+ (●) ratios are plotted against the log of the dose on a log–linear scale. The signals of $C_2F_5^+$, $C_2F_3^+$, and CF_3^+ are normalized to the signal of C^+ at each dose and indicate the degree of fragmentation, unsaturation, and branching in the polymer matrix. The error bars indicate an interval of one standard deviation (±1σ) from the mean. The data are fit by a spline curve as a guide to the eye. The vertical marker designates the maximum level of crosslinking which appears at a dose of $\sim 5 \times 10^9$ Rad.

The notion of increased crosslinking followed by fragmentation as the level of α particle irradiation increases is supported by the observed trends of the $\Sigma C_n/\Sigma C_2$ ratios. Here, ΣC_n refers to a sum of the peaks in the cluster of n carbon atoms, typically $[C_nF_{2n\pm1}]^+$. The C_2 cluster is used as a reference to the C_6, C_5, C_4, and C_3 cluster intensities because the C_2 ions are the monomer fragments and are much less affected by particular stabilization effects. Crosslinking results in a bias of the $\Sigma C_x/\Sigma C_2$ ratio toward the high mass (higher signals in ΣC_x) while fragmentation results in a bias of the $\Sigma C_x/\Sigma C_2$ ratio toward the low mass (higher signals in ΣC_2). The effects of defluorination are marginalized since each sum of clusters includes the defluorinated fragment ion, i.e. $[C_nF_{2n-1}]^+$. The ratios of $\Sigma C_6/\Sigma C_2$, $\Sigma C_5/\Sigma C_2$, $\Sigma C_4/\Sigma C_2$, and $\Sigma C_3/\Sigma C_2$ are plotted in Fig. 9 as a function of α dose on a log–linear scale, and are fit with a spline curve as a guide to the eye. The error bars indicate an interval of one standard deviation (1σ) from the mean. Each curve shows a maxima between 10^9 and 10^{10} Rad followed by a significant decline in the magnitude of the ratio at 5×10^{10} Rad. We conclude, based on these data and the data revealed in the preceding paragraph, that α particle irradiation of the PTFE matrix results in fragmentation, unsaturation and crosslinking at α doses $<10^{10}$ Rad which is followed by extensive fragmentation and further defluorination of the matrix molecules at α doses $>10^{10}$ Rad. In particular, we suggest that the maxima in the curves of $\Sigma C_x/\Sigma C_2$ are attributable to a climax in the level of crosslinking within the α particle irradiated polymer matrix. Some level of fragmentation must occur at α doses $<10^{10}$ Rad to facilitate macroradical diffusion and crosslinking [4,22]. Unsaturation is observed to occur at all levels of irradiation, as evidenced by the data in

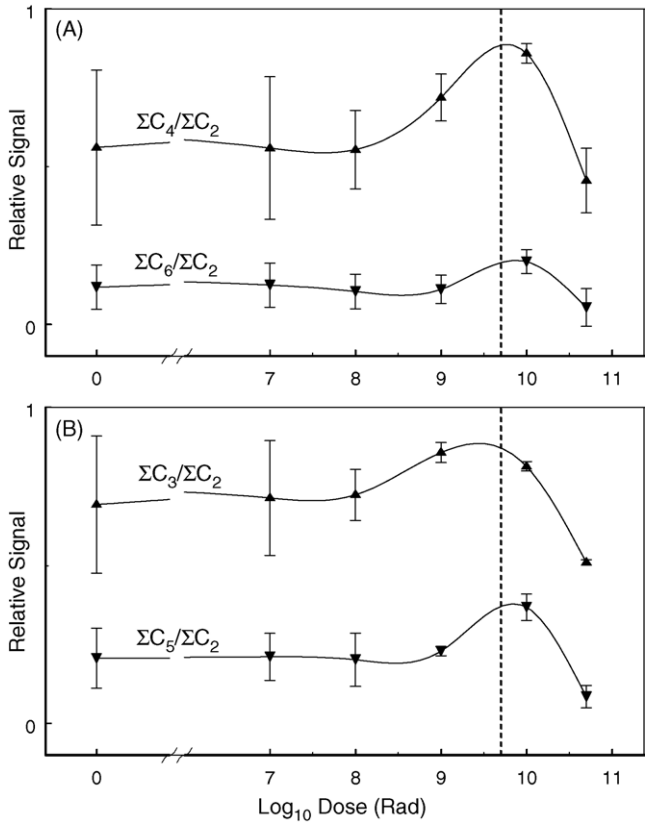

Fig. 9. (A) The magnitudes of the $\Sigma C_6/\Sigma C_2$ (▼) and $\Sigma C_4/\Sigma C_2$ (▲) ratios plotted against the log of the dose on a log–linear scale. (B) The magnitudes of the $\Sigma C_5/\Sigma C_2$ (▼) and $\Sigma C_3/\Sigma C_2$ (▲) ratios plotted against the log of the dose on a log–linear scale. The magnitudes of the $\Sigma C_6/\Sigma C_2$ and $\Sigma C_5/\Sigma C_2$ ratios are multiplied by 3 and 2, respectively. The magnitudes of the $\Sigma C_x/\Sigma C_2$ ratios are sensitive to the level of crosslinking and fragmentation in the polymer matrix as a function of α particle dose. The effects of defluorination and unsaturation are minimized because each sum of clusters includes the defluorinated fragment ion, i.e. $[C_nF_{2n-1}]^+$. The error bars indicate an interval of one standard deviation ($\pm 1\sigma$) from the mean, and the data are fit by a spline curve as a guide to the eye. The vertical markers designate the maximum level of crosslinking which appears at a dose of $\sim 5 \times 10^9$ Rad.

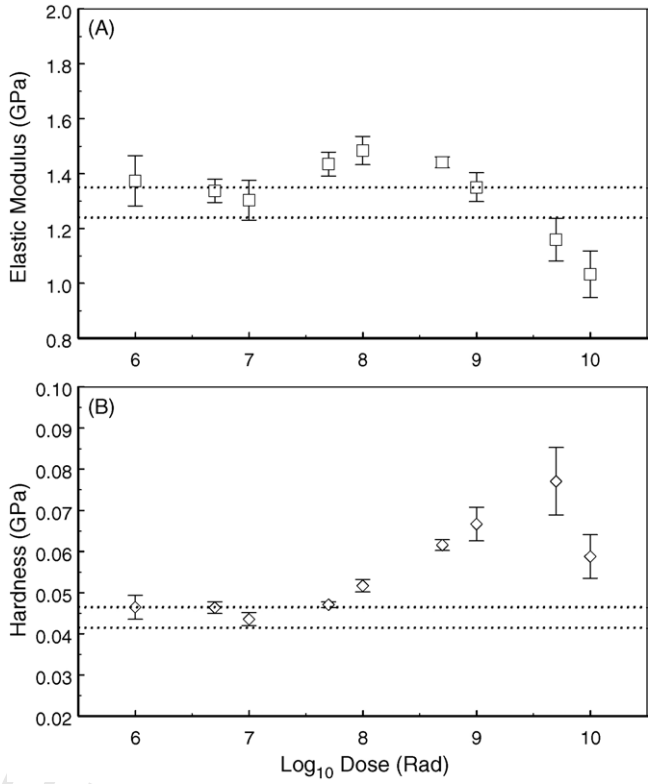

Fig. 10. (A) Elastic modulus of α particle-irradiated PTFE plotted as a function of dose on a log–linear scale. (B) Hardness of α particle-irradiated PTFE plotted as a function of dose on a log–linear scale. The error bars indicate an interval of one standard deviation ($\pm 1\sigma$) from the mean. The dotted lines ($\cdots$) in each graph identify the $\pm 1\sigma$ boundaries from measurements of unirradiated PTFE.

Fig. 4, but escalates with the $F^\bullet$ free radical concentration at higher α doses.

Variation in the mechanical properties of α particle-irradiated PTFE was probed by nanoindentation. The hardness and elastic modulus of PTFE are presented as a function of α dose in Fig. 10. In this figure, the mean values of the hardness and elastic modulus measurements are plotted against the log of the dose. The mean values were calculated from at least four measurements at each α dose; the error bars indicate an interval of one standard deviation (1σ) from the mean. The dashed lines through the plots indicate an interval of one standard deviation for the hardness and elastic modulus values obtained from measurements of unirradiated PTFE. The data show an increase in the hardness of the irradiated PTFE at α doses between 5×10^7 and 5×10^9 Rad that is followed by a drop in hardness. At α doses $\leq 5 \times 10^7$ Rad the hardness is roughly equivalent to that of the unirradiated specimens. Similarly, the data show an increase in the elastic modulus of the irradiated PTFE at α doses between 10^7 and 5×10^8 Rad that is followed by a decline at α doses $\geq 10^9$ Rad. At α doses $\leq 10^7$ Rad the elastic modulus is nearly equivalent to that of the unirradiated specimens. The elastic modulus and hardness are generally sensitive to the average molecular weight and the level of crosslinking, respectively [23]. Therefore, we conclude that scissioning of the linear polymer chains is offset by crosslinking at moderate α doses which leads to a peak in the elastic modulus at 10^8 Rad. The elastic modulus rolls off with continued irradiation due to an increase in molecular mobility that arises by a reduction in the average molecular weight of the matrix molecules (i.e. fragmentation). The magnitude of the hardness shows that crosslinking continues to a dose of 5×10^9 Rad. The hardness declines with continued irradiation due to fragmentation. These conclusions are in general agreement with the ToF-SIMS data which indicate that the level of crosslinking peaks at approximately 5×10^9 Rad, and that fragmentation and branching escalate at α doses $\geq 10^{10}$ Rad.

4. Discussion

There are subtle but obvious disparities between the ToF-SIMS data reported herein which were acquired using a C_{60}^+ ion probe and the data reported earlier [7] which were acquired using a $^{69}Ga^+$ ion probe. Specifically, the tendencies of the $C_2F_5^+/C^+$, $C_2F_3^+/C^+$, and $\Sigma C_x/\Sigma C_2$ ratios demand exploration. With respect to the data acquired using $^{69}Ga^+$ primary ions, the

magnitude of the $C_2F_5^+/C^+$ ratio shows only a minor deviation to the positive at 10^9 Rad that is followed by a significant decline at 10^{10} Rad and, finally, an increase at 10^{11} Rad. The magnitude of the $C_2F_3^+/C^+$ ratio remains relatively constant to $\sim 10^9$ Rad followed by increases at both 10^{10} and 10^{11} Rad. The magnitudes of the $\Sigma C_x/\Sigma C_2$ ratios, for which data were provided for $\Sigma C_4/\Sigma C_2$ and $\Sigma C_3/\Sigma C_2$, follow a trend of decreasing magnitude with increasing α dose. A discernable deviation of the $\Sigma C_4/\Sigma C_2$ magnitude to the positive occurs at 10^{10} Rad. The PTFE specimens are eliminated as a potential source of the observed divergence in the reported data because specimens for all experiments utilizing both the $^{69}Ga^+$ and C_{60}^+ ion probes were cut from the same lot of PTFE sheet stock. The maximum α particle doses are 5×10^{10} Rad and 1×10^{11} Rad for the current (C_{60}^+) and the previously reported ($^{69}Ga^+$) sets of ToF-SIMS data, respectively. However, the slight differences in the maximum experimental α particle doses cannot account for the differences in the data at the lower α doses. The PTFE specimens of each experiment were also irradiated at different dose rates, but our work has shown that there are no discernable differences in the effects of irradiation using dose rates that differ by more than two orders of magnitude (i.e. 0.2–40 nA). This result is due to the nanoampere dose rates used in our experiments that preclude thermal excursions in the sample. Therefore, the apparent irregularities in the data must be explained by the mechanism of secondary ion ejection for the respective primary ion sources employed for data acquisition [24–26]. A brief summary is given here, but the interested reader is directed to the cited articles.

During bombardment of the sample with monatomic primary ions (e.g. $^{69}Ga^+$), emission of analyte species occurs predominantly as a result of direct knock-on collisions via the primary ion-induced linear collision cascade. The calculated temporal evolution of monatomic ion bombardment shows that the incident ions generate a relatively large ion track that is accompanied by a high degree of bond breaking and fragmentation in the sample matrix. The mechanics of monatomic ion bombardment invariably leads to the emission of low mass particles and molecular fragments. During bombardment of the sample with polyatomic primary ions (e.g. C_{60}^+), emission of analyte species occurs predominantly via collective, nonlinear processes. The calculated temporal evolution of polyatomic ion bombardment shows that the incident ions initiate cohesive desorption of molecules which is enhanced by a pressure wave in the sample. In comparison to $^{69}Ga^+$ ion bombardment, C_{60}^+ ion bombardment favors the emission of high mass molecular fragments with less damage imparted to the sample matrix. The advantages of C_{60}^+ ion bombardment include greater sensitivity of both high and low mass ions to structural changes in the PTFE matrix without the detrimental effects of primary ion-induced fragmentation of the analyte species. With respect to the data charted in Fig. 9, a bias in the signals of ions toward higher mass is evident at α doses between 10^9 and 10^{10} Rad and marks a significant structural change in the PTFE matrix. The dissimilarity in the mechanisms of incident $^{69}Ga^+$ and C_{60}^+ ions that lead to emission of analyte species is evident in Fig. 1. The mass spectra of PTFE acquired with a $^{69}Ga^+$ ion probe show a C^+ peak that is consistently prominent, whereas the mass spectra of PTFE acquired with a C_{60}^+ ion probe show a C^+ peak that is consistently minimal. With respect to the data plotted in Fig. 8, the relatively small contribution of the C^+ signals in the denominator of the $C_2F_5^+/C^+$ and $C_2F_3^+/C^+$ ratios causes the magnitudes of these ratios to reflect more accurately the chemical structure of the α particle-irradiated PTFE matrix.

The effects of α particle irradiation are manifested by changes in the chemical structure of PTFE which are corroborated by the physical properties of hardness and elastic modulus as shown in Fig. 10. Low doses of α particles ($<10^9$ Rad) result in scission of the matrix molecules and the formation of relatively labile macromolecular daughters. The increasing concentration of macromolecular daughters generated in the polymer matrix with increasing α particle dose results in crosslinking that reaches a maxima at $\sim 5 \times 10^9$ Rad. Higher doses of α particles ($>10^{10}$ Rad) results in significant fragmentation of both parent and daughter macromolecules which are increasingly branched and unsaturated. These data indicate that the energy deposited into the polymer matrix by MeV α particles occurs by a unique mechanism with consequences that are distinct from other radiation sources.

The majority of experiments reported in the literature concerning the radiolysis of PTFE have been executed using β and γ sources with energies in the keV to MeV range to irradiate the samples [5,6,27–31]. In the cited examples, the chemical properties are probed by infrared spectroscopy (IRS), X-ray diffraction (XRD) or differential scanning calorimetry (DSC) and the physical properties are determined as a function of tensile strength and elongation at break. The results disclosed in these articles show that the chemical structure of PTFE is very sensitive to the incident radiation and the physical properties of the polymer degrade considerably at doses of 10^4 to 10^6 Rad without some form of thermal treatment. Thermal treatments have been shown in most instances to harden the PTFE matrix against the effects of radiation to a dose of $\sim 10^7$ Rad. By contrast, the physical properties of PTFE that has been irradiated with α particles improve to a dose of $\sim 10^{10}$ Rad. The relative instability of PTFE toward β and γ radiation may be understood in terms of the LET of the incident radiation [8].

Irradiation of PTFE with sources of ionizing radiation begets primary (terminal) and secondary (internal) macroradicals by cleavage of C–C and C–F bonds, respectively. Low LET sources such as β and γ radiation result in the generation of isolated reaction centers (i.e. macroradicals). Formation of isolated primary macroradicals via C–C scission is neglected as a significant source of polymer degradation because caging results almost exclusively in geminal recombination of the C–C bonds [4]. Therefore, the formation of secondary macroradicals via C–F scission and the simultaneous production of $F^\bullet$ free radicals is reasoned to be the primary mechanism of degradation in a PTFE matrix irradiated with low LET radiation sources. Since $F^\bullet$ radicals are free to diffuse in the PTFE matrix, it is further reasoned that radiolytically produced secondary macroradicals relax by ejection of another $F^\bullet$ radical

accompanied by the formation of an internal unsaturation. The $F^{\bullet}$ free radicals, in turn, react with C–C bonds of the polymer to generate saturated chain termini (i.e. $–CF_3$), terminal unsaturations (i.e. $–CF{=}CF_2$), and $F^{\bullet}$ radicals. These suppositions are supported by the observed profusion of unsaturations in the polymer matrix as a function of radiation dose [4,32]. In summary, exposure of PTFE to β and γ radiation results in the generation of isolated macroradicals, a circumstance that effectively minimizes the potential for crosslinking, and degradation proceeds via back-biting reactions that stimulate fragmentation and unsaturation of the polymer matrix. The same general outcome is realized upon irradiation of PTFE with neutrons [6].

The ability of a polymer to crosslink depends on macroradicals existing in both spatial and temporal proximity which requires a high LET radiation-polymer interaction [8]. This requirement is satisfied by irradiation of the PTFE matrix with MeV α particles. Notwithstanding, radiation-induced modification of a polymer matrix has been shown by our data [7], and elsewhere [6], to be independent of dose rate. It seems that gas, liquid, and low molecular weight solids are much more sensitive to the effects of dose rate. Moreover, the lifetime of radicals in a PTFE matrix has been shown to be remarkably long [33]. Our data indicate that the requirement for spatial proximity of macroradicals is satisfied at α doses $\geq 10^8$ Rad which corresponds to α particle fluences $\geq 10^{12}$ cm^{-2}. The indicators by which we deduce that crosslinking has taken place are maxima in the magnitudes of the hardness, the $\Sigma C_x/\Sigma C_2$ ratios, and the $C_2F_3^+/C^+$ ratio that appear at an α dose of $\sim 5 \times 10^9$ Rad. Fragmentation and unsaturation are observed to occur at all experimental α doses. However, these phenomena escalate as a function of α dose as a result of the burgeoning $F^{\bullet}$ free radical concentration and surpass crosslinking at doses $\geq 10^{10}$ Rad, corresponding to α particle fluences of $\geq 10^{14}$ cm^{-2}. The markers by which we are able to gauge the level of fragmentation and unsaturation include the magnitudes of the $C_3F_x^+/C^+$, the $C_2F_5^+/C^+$, and the CF_3^+/C^+ ratios. In summary, exposure of PTFE to α radiation results in the production of significant quantities of macroradicals which serve to improve the physical properties of the polymer via crosslinking to a dose of $\sim 10^{10}$ Rad. For the sake of parity, future investigation of the physical properties of α particle-irradiated PTFE should include examination of both tensile strength and elongation. Probing the tensile strength and elongation properties of α-irradiated PTFE will allow for a more direct comparison to data reported for γ-, β-, and n-irradiated PTFE.

While MeV α particles have a limited range of ~27 μm in the PTFE matrix, erosion of the polymer with increasing levels of irradiation is affected by fragmentation, functionalization, and evolution of volatile molecular fragments from the irradiated specimens. Products of radiation-induced reaction between matrix molecules, process additives, residues and intercalated molecular gases are revealed in Figs. 1, 3 and 5, and others have been discussed at length elsewhere [34,35]. The evolution of volatile species has been confirmed by RGA (Fig. 7), and the mass loss that accompanies fragmentation, functionalization, and gas evolution is evident in both the ToF-SIMS (Fig. 5) and the secondary electron (Fig. 6) images. The erosion of the polymer surface that is brought about by the aforesaid processes exposes fresh matrix material to the incident radiation. We speculate that both the hardness and elastic modulus would reach steady state at some α dose greater than 10^{11} Rad. However, experiments directly probing PTFE specimens that have been irradiated at α doses above 5×10^{10} Rad are problematic because the $^{19}F(\alpha,n)$ reaction (i.e. $^{19}F + \alpha \rightarrow {}^{22}Na + n$) results in a significant yield of MeV neutrons.

5. Conclusions

The use of a C_{60}^+ ion probe during ToF-SIMS analysis of the PTFE specimens presents several advantages over the use of a $^{69}Ga^+$ ion probe. We have observed a 500-fold increase in the signal which is attained by a multiplication of 50 in total ion counts using an order of magnitude less total ion dose. Higher mass resolution has enabled more rigorous identification of isobaric species. The increases in signal and mass resolution, together with the minimization of charging artifacts, have facilitated the assignment of fragments beyond 300 *m/z*. The acquisition of ion-specific images with which to identify chemical features and trends in the mass spectra as a direct consequence of α particle irradiation has also been facilitated.

Chemical degradation and mass loss in the surface region is the mechanism of failure in PTFE that has been irradiated with α particles to high doses. The ToF-SIMS data show that chemical degradation occurs by fragmentation, unsaturation, and functionalization of molecules in the polymer matrix. Radiolytic decomposition of the polymer matrix results in evolution of volatile molecules from the surface as revealed in the RGA data. This loss of matrix material is revealed in the total ion images acquired by ToF-SIMS and is further illustrated in the SEM images.

In general agreement with our previous work, we conclude that α particle irradiation of PTFE results predominantly in crosslinking at doses $<10^{10}$ Rad which is accompanied by lesser levels of fragmentation, branching, and unsaturation. In fact, the apex in the observed level of crosslinking occurs at $\sim 5 \times 10^9$ Rad which is the quantity of irradiation where we observe a peak in the hardness. Scission is a constant factor throughout the irradiation regime promoting macromolecular diffusion, crosslinking, unsaturation, and branching. However, at α doses $\geq 10^{10}$ Rad the extent of fragmentation, branching, and unsaturation becomes extreme and is clearly accompanied by the unrestrained growth of radiation-induced products of reaction between matrix molecules, process additives, residues, and intercalated molecular gases. Moreover, both the hardness and elastic modulus decline at α doses $\geq 10^{10}$ Rad. Thus, an exposure limit of $\sim 10^{10}$ Rad is recommended for nominal retention of functional molecular structure and functional physical properties. The room temperature exposure limit for α radiation is roughly 4–6 orders of magnitude greater than the exposure limit for γ, β, and n radiation. Thus, we have shown

definitive evidence that the concept of "equal energy, equal damage" is incorrect.

Acknowledgements

G.L. Fisher would like to acknowledge the assistance of Chad Meserole for critical discussions and review of this manuscript. Financial support for this research was provided by the United States Department of Energy under contract number W-7405-ENG.

References

[1] T. Rollow, Type A Accident Investigation of the March 16, 2000 Plutonium-238 Multiple Intake Event at the Plutonium Facility, Los Alamos National Laboratory, New Mexico, United States Department of Energy, Office of Oversight, Safety and Health, 2000.
[2] A. Charlesby, Atomic Radiation and Polymers, Pergamon, New York, 1960.
[3] B.J. Lyons, Radiat. Phys. Chem. 45 (1995) 159.
[4] J.S. Forsythe, D.J.T. Hill, Prog. Polym. Sci. 25 (2000) 101.
[5] W.W. Parkinson, W.K. Kirkland, The Effect of Air on the Radiation-Induced Degradation of Polytetrafluoroethylene (Teflon), ORNL-1757, Oak Ridge National Laboratory, Oak Ridge, 1967.
[6] J.G. Carroll, R.O. Bolt, Nucleonics 18 (1960) 78.
[7] G.L. Fisher, J.A. Ohlhausen, C.J. Wetteland, Surf. Int. Anal. 37 (2005) 713.
[8] E.H. Lee, Nucl. Instrum. Methods Phys. Res. B151 (1999) 29.
[9] R.M. Braun, P. Blenkinsopp, S.J. Mullock, C. Corlett, K.F. Willey, J.C. Vickerman, N. Winograd, Rapid Commun. Mass Spectrom. 12 (1998) 1246.
[10] D. Weibel, S. Wong, N. Lockyer, P. Blenkinsopp, R. Hill, J.C. Vickerman, Anal. Chem. 75 (1754).
[11] D. Briggs, Surf. Int. Anal. 15 (1990) 734.
[12] W.C. Oliver, G.M. Pharr, J. Mater. Res. 7 (1992) 1564.
[13] J.G. Newman, B.A. Carlson, R.S. Michael, J.F. Moulder, Static SIMS Handbook of Polymer Analysis, Physical Electronics, Eden Prairie, 1991 .
[14] D. Briggs, Surf. Int. Anal. 14 (1989) 209.
[15] A.B. Ariawan, S. Ebnesajjad, S.G. Hatzikiriakos, Powder Technol. 121 (2001) 249.
[16] A.B. Ariawan, S. Ebnesajjad, S.G. Hatzikiriakos, Polym. Eng. Sci. 42 (2002) 1247.
[17] R. Michael, D. Stulik, Appl. Surf. Sci. 28 (1987) 367.
[18] M. Leleyter, J. Phys. 48 (1963).
[19] A.A. Galuska, Surf. Int. Anal. 25 (1997) 790.
[20] F.W. McLafferty, F. Turecek, Interpretation of Mass Spectra, University Science Books, Mill Valley, 1993.
[21] W.J. van Ooij, R.H.G. Brinkhuis, Surf. Int. Anal. 11 (1988) 430.
[22] N.M. Bol'bit, V.B. Taraban, E.R. Klinshpont, I.P. Shelukhov, V.K. Milinchuk, High Energy Chem. 34 (2000) 272.
[23] E.H. Lee, G.R. Rao, L.K. Mansur, Trends Polym. Sci. 4 (1996) 229.
[24] Z. Postawa, Appl. Surf. Sci. 231–232 (2004) 22.
[25] S. Sun, C. Szakal, E.J. Smiley, Z. Postawa, A. Wucher, B.J. Garrison, N. Winograd, Appl. Surf. Sci. 231–232 (2004) 64.
[26] R. Kersting, B. Hagenhoff, F. Kollmer, R. Mollers, E. Niehuis, Appl. Surf. Sci. 231–232 (2004) 261.
[27] J. Sun, Y. Zhang, X. Zhong, Polymer 35 (1994) 2881.
[28] X. Zhong, L. Yu, W. Zhao, Y. Zhang, J. Sun, Polym. Degrad. Stab. 41 (1993) 223.
[29] S. Abdou, R.I. Mohamed, J. Phys. Chem. Sol. 63 (2002) 393.
[30] U. Lappan, U. Geiβler, L. Hauβler, D. Jehnichen, G. Pompe, K. Lunkwitz, Nucl. Instrum. Methods Phys. Res. B185 (2001) 178.
[31] W. Burger, K. Lunkwitz, G. Pompe, A. Petr, D. Jehnichen, J. Appl. Polym. Sci. 48 (1973).
[32] U. Groβ, P. Dietrich, G. Engler, D. Prescher, J. Schulze, K. Lunkwitz, A. Ferse, J. Fluor. Chem. 20 (1982) 33.
[33] Z.X. Zhen, Radiat. Phys. Chem. 35 (1990) 194.
[34] G.L. Fisher, C. Szakal, C.J. Wetteland, N. Winograd, J. Vac. Sci. Technol., submitted for publication.
[35] G.L. Fisher, C. Szakal, C.J. Wetteland, N. Winograd, J. Phys. Chem., submitted for publication.